# Morphology of polymeric powders in Laser Sintering (LS): from Polyamide to new PEEK powders

**S Berretta, O Ghita and K E Evans**

*University of Exeter, College of Engineering, Mathematics and Physical Sciences, EX4 4QF, Exeter, United Kingdom*

***Corresponding author***
Silvia Berretta: sb508@exeter.ac.uk

***Abstract***
In an attempt to expand the range of engineering polymers used for laser sintering, this paper examines the morphology, flowability and interparticle interactions of two commercially available poly (ether ether) ketone (PEEK) powders, not yet optimised for the LS process, by comparison with the LS optimised Polyamide (PA) and Polyetherketone (PEK) powdered polymers . The effect of incorporating fillers and additives on the flow behaviour is also analysed. The Particle Size Distribution (PSD) results alone do not allow ranking the powder materials in relation to the flow behaviour. The particle morphology has a stronger influence on the flow characteristics for materials with similar PSDs. The work also provides additional characterization parameters to be considered when analysing LS powders.

***Graphical abstract***

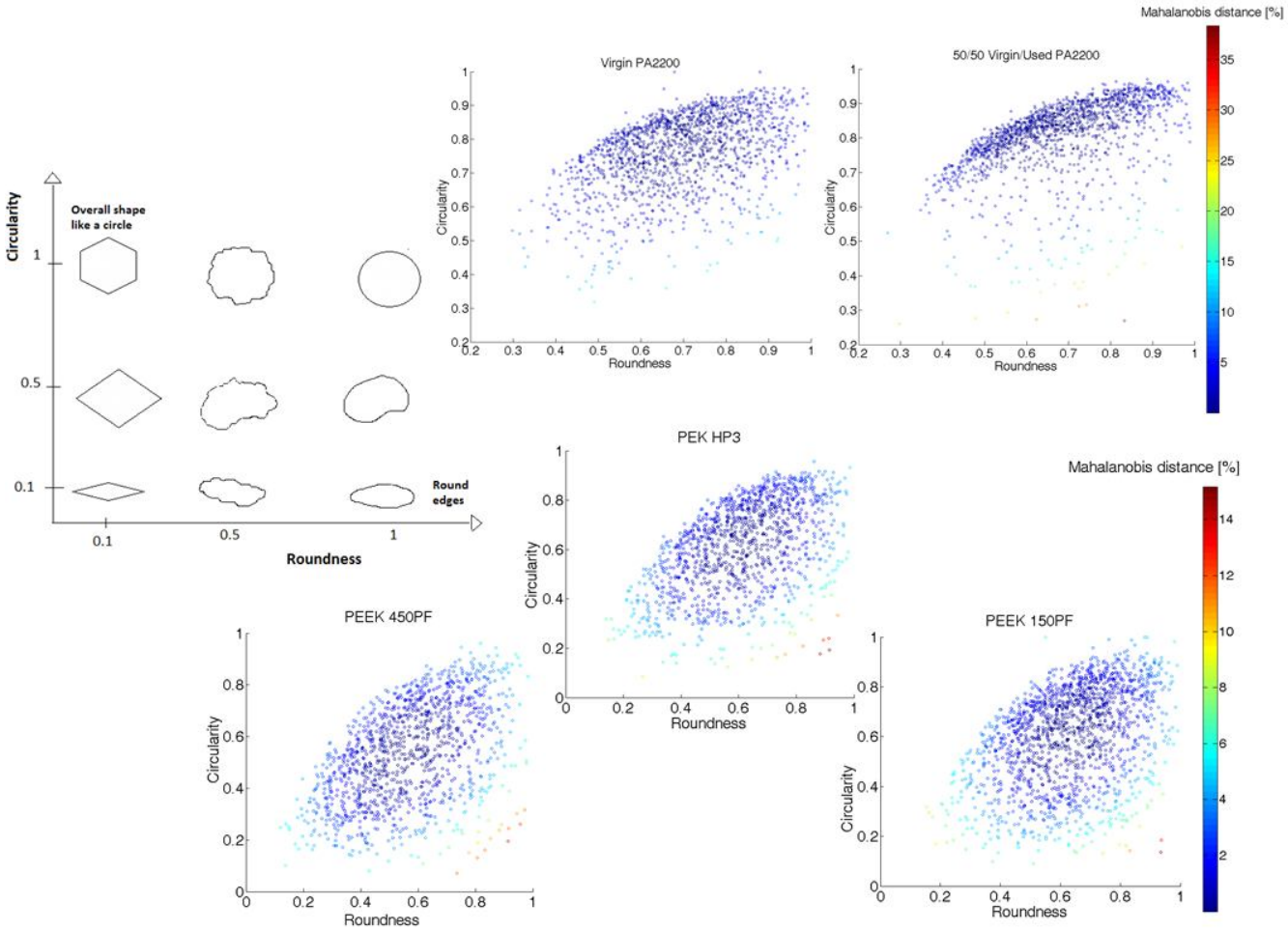


***Keywords***

Laser sintering, particles, morphology, polyetheretherketone, flow.

## *1. Introduction*

Laser Sintering (LS) is a technology commonly used in the additive manufacturing (AM) sector for manufacturing polymeric parts. The technique builds, layer upon layer, three dimensional objects by selectively sintering polymeric powders. The quality (i.e. the detailed resolution, mechanical integrity and dimensional stability) is determined both by the building process and the properties of the original powder. Over the years, most polymeric LS research has focussed either on the manufacturing process

or on the characterization of the final sintered parts [1-6]. Very little attention has been given to the raw powders, their influence on the sintering process and ultimately their relationship with the part properties. Whereas the behaviour of polymeric materials has been fully investigated for other conventional manufacturing processes such as rotational moulding and cold compaction [7, 8], a thorough analysis into the optimum properties of additive manufacturing powders is missing. The aim of this paper therefore, is to investigate the morphological characteristics of a range of powders and their ability to flow to help to understand critical parameters and requirements when developing new medical grades of powders for LS.

Flowability plays a key role in the LS process as the lack of homogeneous and even layers leads to porous, weak LS parts [4, 9]. Flowability depends on several factors: the powder itself (particle size distribution, particle shape, particle surface features); the environmental conditions (temperature, moisture) and according to some authors, to the flow test adopted (angle of repose, Carr Indices, compressibility, etc.) [10, 11]. Schulze [11] reports the basic concepts about bulk solid materials and flowability and he describes the main physical factors affecting flowability, such as adhesive strength and wall friction. Prescott and Barnum [10]suggest distinguishing between “powder flow properties” and “powder flowability”. Powder flow properties are defined by the interactions between the individual particles and affect the flow performance: powder density, compressibility, cohesive strengths within the particles and wall friction. Powder flowability instead refers to how a given material will flow in specific equipment, implying that the same material will behave differently in different flow equipment conditions. In this case, it is largely recommend using a test able to simulate as closely as possible the flow in the real scenario, using the equipment which will be ultimately used for manufacturing. Clearly, the two methods of defining powder flow properties (stand-alone tests or real scenario test) are not particularly satisfactory because they outline the lack of a general method able to precisely predict the flowability of a material under any conditions when its flow properties are known.

In LS, powders have to provide high density, surface quality and accuracy in the final parts, therefore finer powders are preferred. However, negative effects typical of fine particles are sometimes encountered e.g. poor flow, agglomeration, undesired sintering [4, 12], difficulty to remove the unsintered powder from the manufactured products or fogging of the optical elements inside the system[13].

Build layer thickness in LS is approximately 100-150μm [4]. Therefore, in order to ensure that the powder fusion occurs at direct contact of the laser on the particle rather than relying on particle-to-particle conduction, the layer thickness is recommended to be at least two times the size of the particle average size. However, each research study discussing particle size distribution for additive manufacturing claims a slightly different range: sometimes they overlap, other times they are

significantly different. Foderhase et al. [14] studied nylon based composites, either reinforced with glass fibers with lengths of 70 and 85µm or glass beads with diameters ranging from 4 µm to 114µm. Analyses of the LS nylon glass bead composites (29% glass concentration in volume) outlined the difficulty of spreading and the poor flow performance of the mixtures containing 4 µm and 11 µm particles. According to the authors, the reasons were due to interparticle friction which is higher between the smaller particles, especially at high temperatures. Chang et al. [15] claim that in general particles in the range 10-150 µm are preferred, on the basis that the powder size distribution (PSD) has to be slightly smaller than the layer thickness of the LS equipment used. In their case, a Sinterstation 2000 (3D Systems, USA) with layer thickness lying in the range 100-200 µm was used and therefore the authors considered materials with PSD ranging 10-150 µm to be suitable. Drummer et al. [16] report that commercial LS good flowing materials have an average particle size of 60 µm with low presence of particles of diameter equal to, or less than 10 µm. Gibson and Shi [17] mention the particle size as one of the factors affecting the laser depth penetration during LS. Xiao et al. [18] developed a new bioactive glass–ceramic apatite–wollastonite (A–W) powder for indirect laser sintering with PSD in the range of 45-90µm without discussing their choice. Goodridge et al. [4] state as ideal for LS the particle size range of 45-90µm with the suggestion to avoid particles smaller than 45µm but no experimental data are provided to support it . Works using bigger irregular particles are also mentioned. McAlea et al. [19]patented a method (spray drying and air classification) for the production of optimal powders for LS which leads to nearly regular and round particles with a PSD characterized by an average particle diameter between 20 and 50µm, less than 5% (by volume) of particles with size smaller than 15 µm, and less than 2%(by volume) of particles having size greater than 75µm. The authors explain that smaller particles may cause: gashes and fissures when spread on a previously sintered layer, high in-plan shear forces because of interparticle friction and undesired sintering. Hao et al. [20] sintered two classes of specimens in compounded 20% Hydroxyapatite (HA)- HDPE, one with PSD ranging 0-105 µm and one with PSD greater than 105 µm. The first showed a portion of particles which were relatively spherical, while the second class was characterised by very irregular particles. By analysing the mechanical properties, the surface roughness and the porosity of the LS parts, the authors demonstrated that larger particles led to higher surface roughness, and larger and more surface pores in the sintered samples than in the ones sintered with smaller particles. Furthermore the percentage of internal pores increased with higher particle size. It is important to outline that several researchers reported the use of nanoparticles as additives [15, 16, 21-23], although no further details on expected behaviour on particle flow were given.

Regarding flow analysis in LS, the research is limited or again more focussed on the final part properties. Goodridge et al. [4] report that a good flow behaviour is achieved with spherical or nearly spherical particles. Van der Schueren et al. [24] seem to confirm such hypothesis by the analysis of three deposition methods in selective metal sintering. They state that the flow is mainly influenced by

the inter-particle friction and the spherical shape of particles ensures the minimal contact between particles causing a reduction in friction. Dupin et al. [25] studied two types of LS polyamide 12: Duraform PA (3D systems, USA) with median particle size of 60 µm and high frequency of small diameter particles (8 µm) and Innov PA (Exeltec, France) with median diameter of 43µm and more regular and rounder particles than Duraform PA particles; and used 1% silica in both materials to improve the flow performances. The authors then discussed optimal particle properties by studying the mechanical part properties. More precisely, they found that Duraform PA gave less porosity than Innov PA in the sintered specimens, even at lower energy density. In other words the irregular shaped particles with broader PSD and significant presence of small particles of Duraform PA led to better properties in the final parts than spherical particles with narrower PSD (Innov PA). Lastly, Amado et al.[26] focussed on the characterization of laser sintering powders by using a well-established powder analyser apparatus based on a rotational drum and an image acquisition system. Nine types of powders of different chemical nature, obtained through different methods, were exhaustively analysed in terms of flow and fluidized behaviours. The materials characterized by nearly spherical particles and the ones composed by convex shape particles showed higher performances in: flow behaviour, packing density and capacity to achieve a fluidized state, while the materials composed by less regular geometry shaped particles and especially flake like powders presented: poorer flow and packing density, small fluidization tendency with additional complexity such as dilatancy. According to the authors, good flow, high packing density and a high rate to reach a fluidization state constitute the ideal characteristics of a LS material. Interestingly, if the fluidization tendency is very high, the speed of the powder delivery system must be lowered to avoid a poor bed density.

As can be seen above, although various studies have touched upon the powder requirements for the LS process, most of them lack a clear and quantitative evaluation of the raw materials, while some studies give a qualitative assessment.

## *2. Experimental work*

### *2.1 Materials*

The materials analysed here have been divided for clarity into four groups: (1) standard LS grades; (2) new grades, non LS powders; (3) fillers; and (4) additives.

#### *2.1.1 Commercial LS grades*

The LS commercial grades were PA2200 and HP3, both supplied by EOS e-manufacturing solutions (EOS, Germany )[27]. HP3 is a Polyetherketone (PEK) polymer, i.e. a high temperature thermoplastic, belonging to the chemical family of polyaryletherketones (PAEKs), known for its high mechanical properties, elevated thermal stability and outstanding chemical resistance[28]. PA2200 is a polyamide 12 polymer. Pure virgin PA2200 and a mixture by weight of 50% virgin and 50% used material (unsintered powder that has gone through one building process) were used in this study. Mixtures of PA2200 including 50% by weight used material is generally accepted and frequently used commercially in LS.

*2.1.2 New high temperature non-LS grades*

Two grades of PEEK traded under the name of VICTREX® PEEK 450PF and VICTREX PEEK 150PF, produced by Victrex Polymer Solutions [29], constitute the new potential powders for LS systems. As belonging to PAEKs, these materials are also high temperature thermoplastics with high mechanical performances, excellent chemical and thermal stability. In addition, PEEK is biocompatible. The main difference between VICTREX® PEEK 450PF and VICTREX® PEEK 150PF is the melt viscosity, determined as 350 Pa.s and 130 Pa.s, respectively [29].

*2.1.3 Fillers*

The fillers utilized for this study were glass, hydroxyapatite and calcium carbonate. The glass powder was a LS grade commercially known as Spheriglass 2000 (supplied by Potters[30]). Hydroxyapatite (HA) was supplied by Sigma-Aldrich[31] and used because of its biocompatible and bioactive characteristics . Calcium carbonate ($CaCO_3$) (supplied by Ash Grove Cement Company[32], KS) was selected due to its smaller particles size. These fillers were added to PEEK 450PF in the following percentages by weight: 450PF/Spheriglass (90:10); 450PF/Spheriglass (80:20); 450PF/Spheriglass (70:30); 450PF/HA (80:20); 450PF/HA (70:30); 450PF/ $CaCO_3$ (90:10); 450PF/$CaCO_3$ (80:20); 450PF/$CaCO_3$ (70:30).

*2.1.4 Additives*

Aerosil 200Pharma, supplied by Evonik[33], was used in this investigation. This is a nano silica powder designed for improving the flow in pharmaceutical products[33]. The following mixtures were prepared using a high speed mixer: 450PF /Aerosil (99:1) and 150PF/Aerosil (99:1) (by weight).

### ***2.3*** *Particle Size distribution (PSD)*

The particle size distributions of 50/50 virgin/used PA2200, PEK HP3 and PEEK grades were determined using a Saturn DigiSizer 5200 (Micromeritics, US). The instrument gives the particle size distribution of a sample by detecting its light scattering pattern when the specimen is suspended in a specific solution. Here, a solution of 0.4% sodium hexametaphosphate (more precisely, 6.7g sodium hexametaphosphate and 1.3g sodium hydrogen carbonate for 2L deionized water) was used. The analysis of PA2200 was carried out using Malvern Instruments MASTERSIZER supported by MICROPLUS Version 2.19 software, with the same test conditions. All the tests were repeated three times on each sample and the average results of the three repeats are reported here.

### *2.4 Scanning Electron Microscopy (SEM)*

SEM examination was performed with a Hitachi S-3200N scanning electron microscope. The samples were coated with 4nm of gold coating in order to reduce the surface charging and the electron secondary imaging was set with an accelerating voltage of 25kV.

### *2.5 Particle Shape Analysis*

The shape analysis was carried out by using the image processing program “Image J”[34].The software is capable of evaluating shape descriptors on specimen images. SEM images were used and processed according to the following procedure: setting of the scale, conversion to binary image, drawing the edges of particles using the automatic wand and the freehand tool, evaluation of the shape parameters through the ROI manager window. The particles analysed were not overlapping and not lying on the edges of the image. Circularity, Roundness, Aspect Ratio (AR) and Solidity were the shape descriptors evaluated for all the powder samples [34]. The shape analysis was carried out on HP3 PEK, virgin PA2200, 50/50 virgin/used PA2200, PEEK 450PF and PEEK 150PF. The numbers of particles evaluated for each grade were: 1174, 1538, 1539, 1154 and 1498, respectively.

### *2.6 Angle of Repose (AOR)*

Angle of Repose (AOR) is a single-point test which quantifies the angle of a cone of bulk material over a flat surface assuming that each material has its own specific angle of repose. The cone is formed by dropping the material through a funnel of standardized dimensions and the angle

considered is the inner one formed between the slant height and the horizontal plane. The smaller the angle of repose is, the higher the flowability is. The test was designed by following the ASTM C144 standard [35]. The interior of the glass funnel was covered with paper in such a way to fit perfectly the angle of the funnel and to facilitate the flow of powder; the powders were added in small amounts; the powder was supplied through the funnel until the cone of deposited material reached the tip of the nozzle. The test was repeated six times on each material.

*2.7 Evaluation of the Hamaker constant*

Powder materials can be cohesive or free flowing due to different factors such as particle morphology, size, chemical nature and interacting medium[36]. Van der Waals' forces are often taken into account to evaluate the intermolecular interactions responsible of macroscopic properties between the particles of a given material [37]. In this scenario, the Hamaker constant is a force constant able to predict or estimate the interparticle interactions by considering the physic-chemical nature of the materials involved [38-42]. In general, in the interaction of two spheres, the smaller the Hamaker constant is, the smaller the Van der Waals' forces are likely to be[43] and therefore the better the particles will flow. The Hamaker constant can be estimated by two methods: Hamaker's and Lifshitz'. Lifshitz' [44] theory is more rigorous and overcomes limitations of Hamaker's approach by treating the bodies as continua. The calculation is done by using the refractive indices and the dielectric constants of the powder materials involved, and the ones of the medium in which they interact [43]. Equation 1 presents the Hamaker constant according to Lifshitz' formula. $K_B$ is the Boltzmann constant ($K_B = 1.38 \cdot 10^{-23}\ \frac{J}{K}$); T is the temperature ($T = 300\ K$); h represents the Plank's constant ($h = 6.63 \cdot 10^{-34}\ J \cdot s$); $\upsilon_e$ is the electron orbiting frequency ($\upsilon_e = 3 \cdot 10^{15} Hz$); $\varepsilon_1$, $\varepsilon_2$, $\varepsilon_3$ are the dielectric constant of phase 1, 2 and interacting medium respectively; $n_1$,$n_2$,$n_3$ are the refractive indices of phase 1, 2 and interacting medium, respectively. Phase 1 and Phase 2 are the powder materials utilised, while medium is air.

Values of refractive indices and dielectric constants were taken from the available literature [29, 33, 45-50].

$$A \approx \frac{3}{4} K_B T \left(\frac{\varepsilon_1 - \varepsilon_3}{\varepsilon_1 + \varepsilon_3}\right)\left(\frac{\varepsilon_2 - \varepsilon_3}{\varepsilon_2 + \varepsilon_3}\right) + \frac{3}{8}\frac{h\upsilon_e}{\sqrt{2}} \frac{(n_1^2 - n_3^2)(n_2^2 - n_3^2)}{\sqrt{(n_1^2 + n_3^2)}\sqrt{(n_2^2 + n_3^2)}\left\{\sqrt{(n_1^2 + n_3^2)} + (n_2^2 + n_3^2)\right\}}$$

**Equation 1**. Hamaker constant A.

## *3. Results and discussion*

### *3.1 Particle Size Analysis*

The particle size distributions (PSD) of LS grade powders (HP3 PEK, virgin PA2200 and 50/50 virgin/used PA2200) and non LS ones (PEEK 450PF and 150PF) are reported in figure 1.

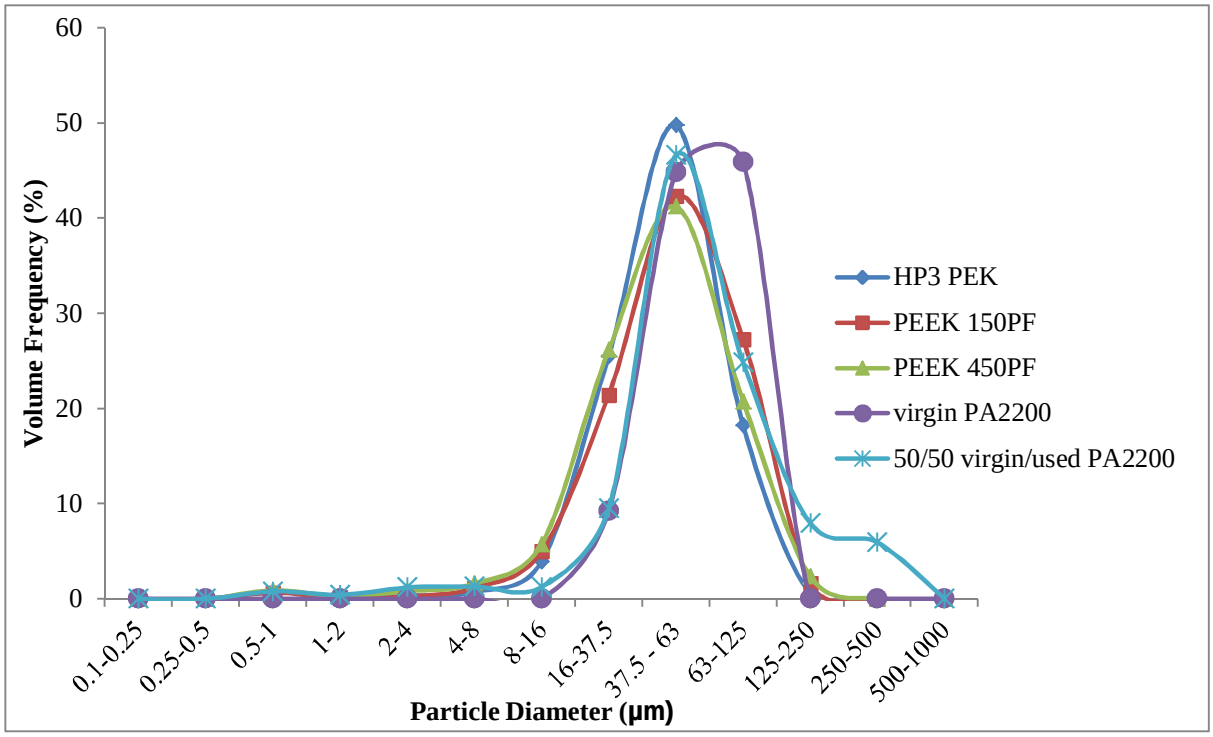


**Figure 1**. PSD of LS grades and new materials for LS.

HP3 PEK and both PEEK grades exhibit fairly similar PSDs, covering approximately the same diameter range. However, HP3 PEK shows a higher content of particles having a diameter of 63µm. PA2200 curve is slightly shifted to the right, indicating the presence of particles with larger diameters than the other grades. The PSD of 50/50 virgin/used PA2200 was similar to that of the PAEK powders.

PSD data for fillers used with PEEK 450PF are shown in figure 2.

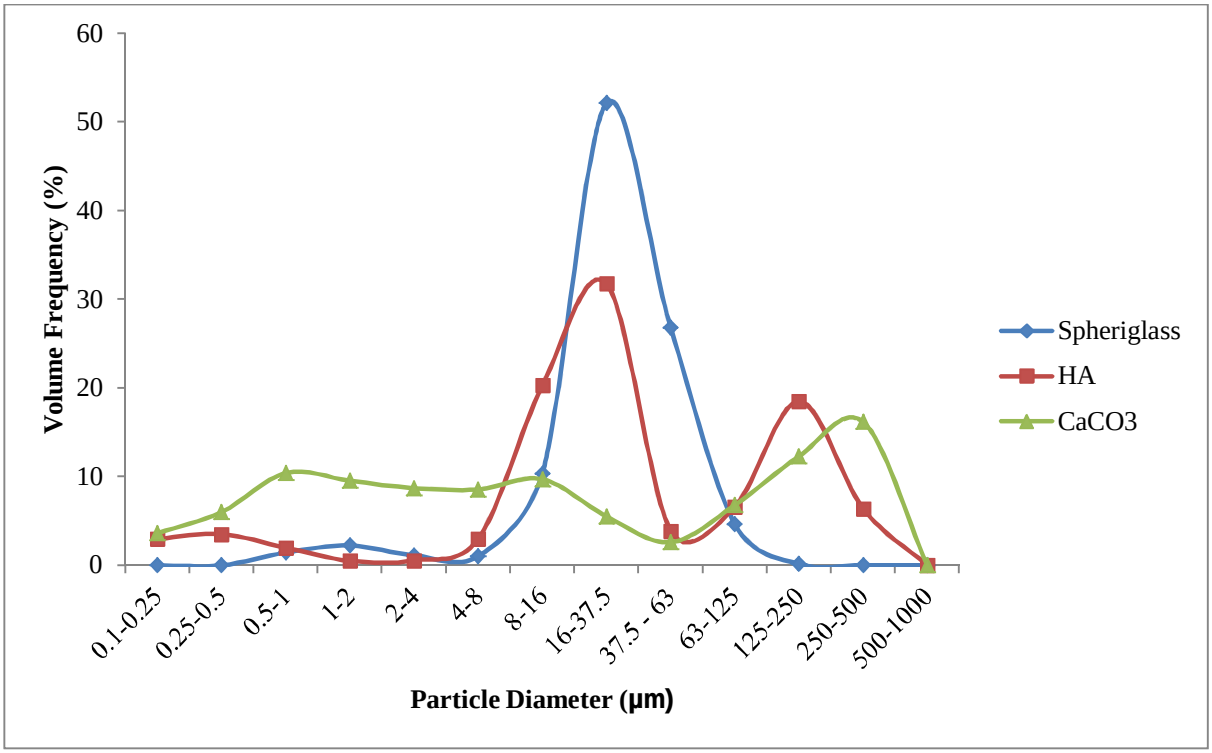


**Figure 2.** PSD of fillers.

The powders show very different distributions. Calcium Carbonate ($CaCO_3$) shows fairly constant amount of particles along all the particle diameters. HA exhibits a bimodal distribution with peaks for diameters at which PEEK 450PF has fewer amounts of particles. Spheriglass presents a similar PSD to those of PEEK materials, but with a higher content of smaller particles: this could be good as a wider range might allow a better compaction of the powder during the spreading stage in the LS process.

### *3.2 Particle morphology*

#### *3.2.1 Commercial SLS grades*

The particle morphologies of PA2200 and 50/50 virgin/used blend powders at three orders of magnifications are reported in figure 3 and 4. The particles look circular or slightly elongated, round with smooth but cracked surface in both materials. As PA2200 represents a well-established LS material, its morphology has been considered the benchmark for the other materials analysed here.

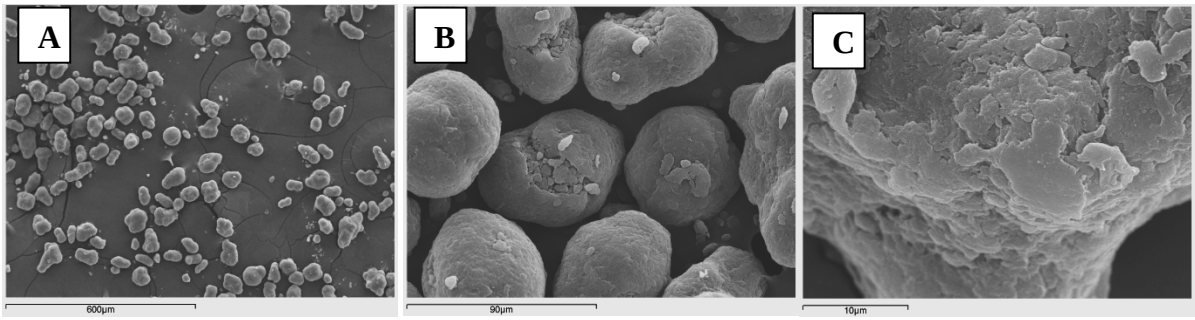


**Figure 3.** Virgin PA2200 at low (A), medium (B), and high (C) magnification.

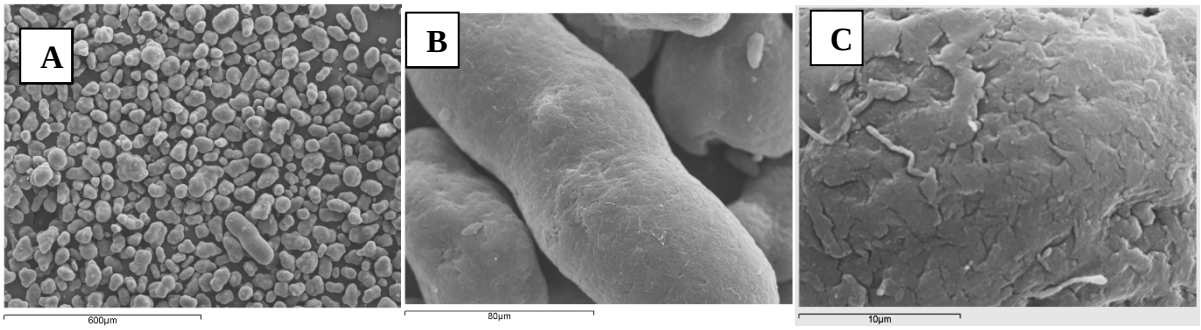


**Figure 4.** 50/50 virgin/used PA2200 at low (A), medium (B), and high (C) magnification.

HP3 PEK, which has been recently introduced to the LS market, contains particles which are not as round as PA2200 particles, though they exhibit smooth surfaces and fully dense structures (figure 5).

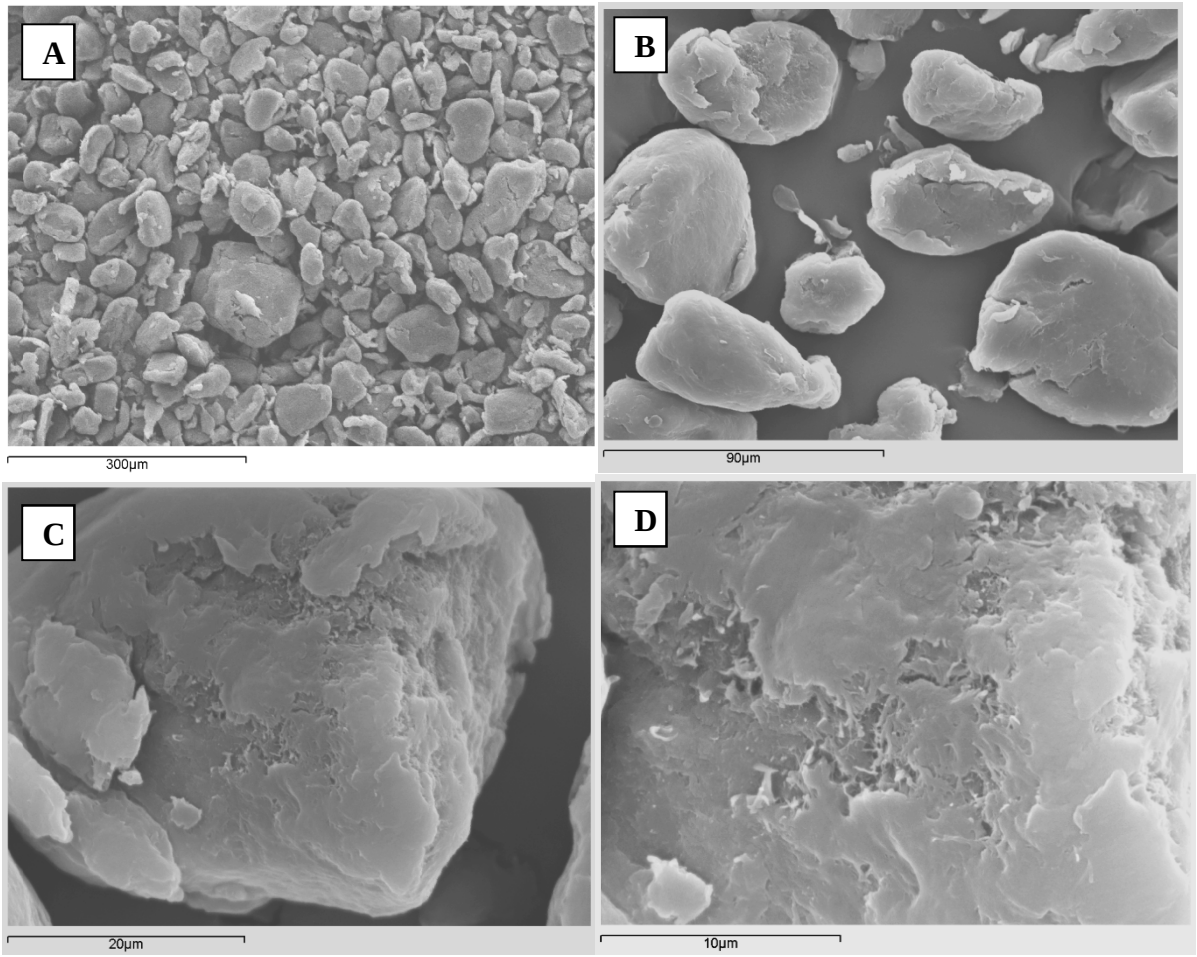


**Figure 5.** HP3 PEK low (A), medium (B), and high (C, D) magnification.

### *3.2.2 New high temperature non –LS grades*

Particles of both PEEK grades are shown in figures 6 to 8. More precisely, figure 6 shows the angular particles of PEEK 450PF, also characterized by the presence of highly irregular flaky structures on the surfaces. These flakes and fibrils did not appear in the values of circularity and roundness from the shape analysis in Image J as the software cannot detect on surface irregularities if they do not lie on the external edge of a particle (Fig.7). Furthermore, PEEK 450PF particles appear not fully dense (Fig. 6 D). Figure 8 shows the particles of PEEK 150PF.It is interesting to note that this material includes two types of structures: the structure A is similar to the flaky one found for PEEK 150PF (Fig. 8, C and D); the structure B is characterized by round protuberances composed by fibril substructures (Fig. 8, E and F). The authors believe that as the structure B appears rounder in shape at larger scale, it is responsible for the better performance of PEEK 150PF when compared to PEEK 450PF, as outlined in the shape analysis.

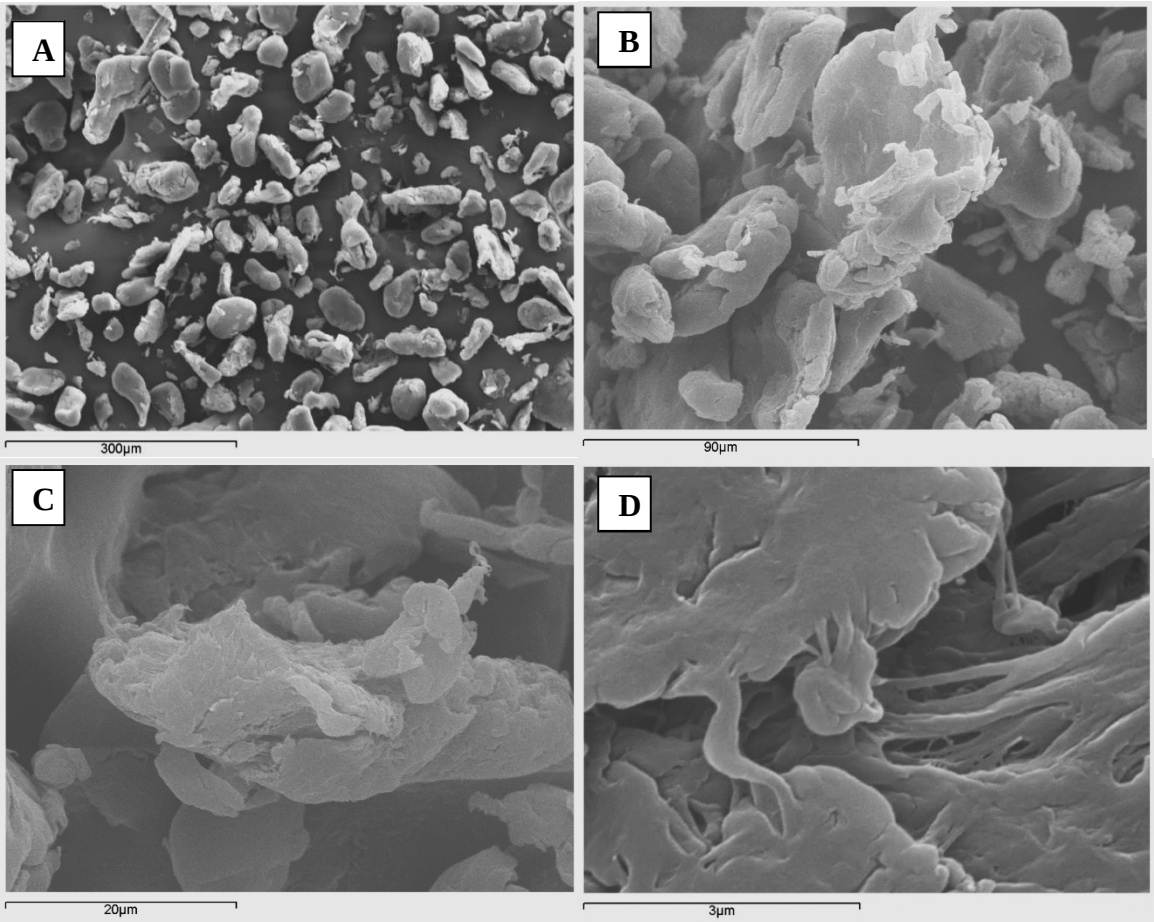


**Figure 6.** PEEK 450PF at low (A), medium (B, C) and high (D) magnification.

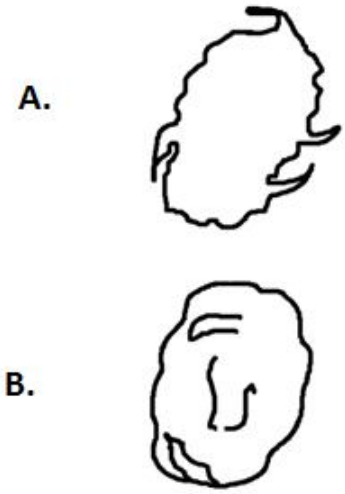


**Figure 7.** Particle surface features in the shape analysis: flakes that affect the shape parameters (A) and flakes that do not affect the shape descriptors (B).

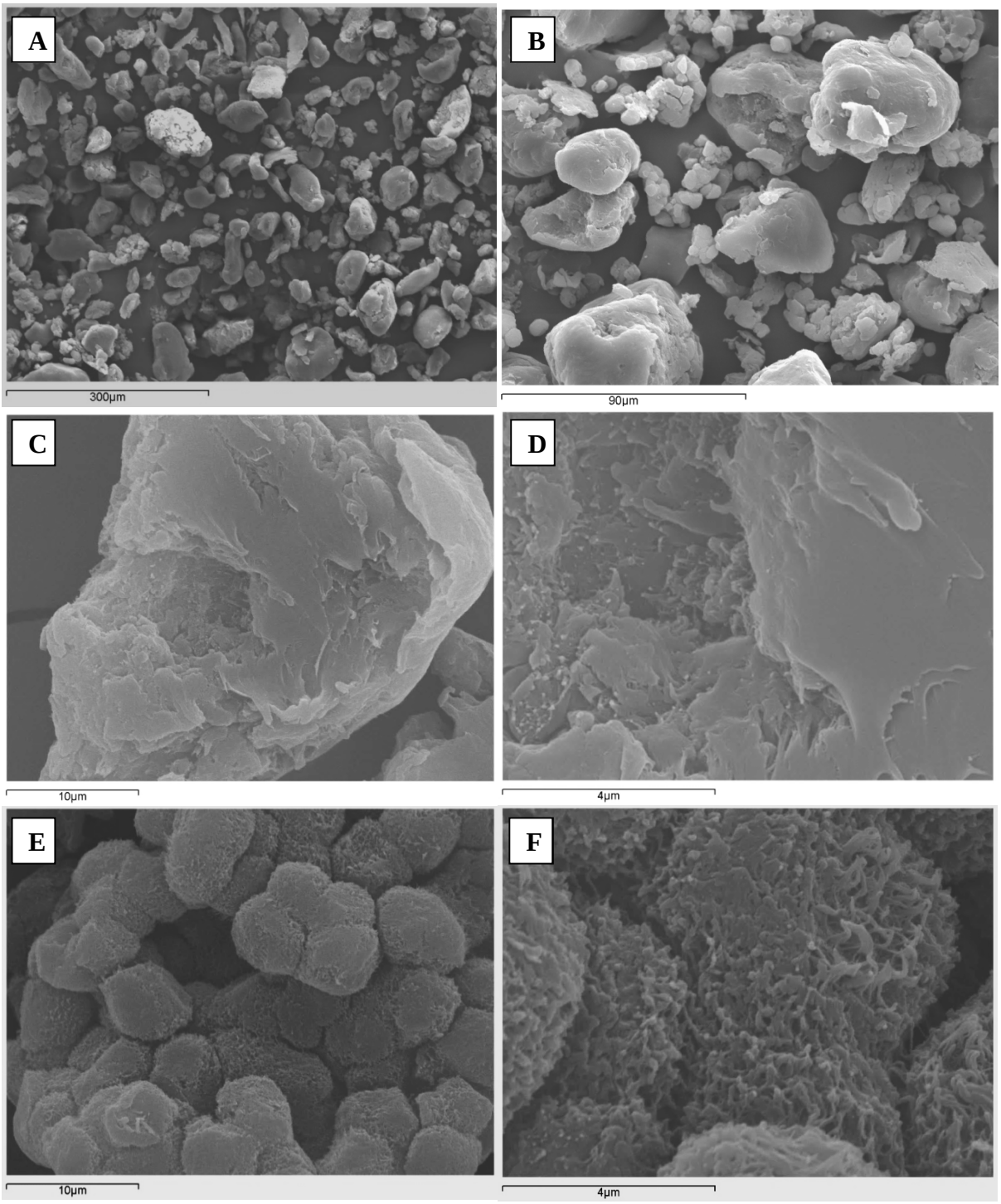


**Figure 8.** PEEK 150PF, at low (A) and medium (B) magnification. Structure A (C, D). Structure B (E, F).

### *3.2.3 Fillers*

Spheriglass particles are mostly round, smooth and fully dense (Fig. 9,A ), while Calcium Carbonate (Fig. 9,B) as noticed also from the PSD, contains also much smaller particles than the LS grades and

other fillers. $CaCO_3$ particles also seem to agglomerate. HA particles are round with quite complex nano-structures (Fig. 10).

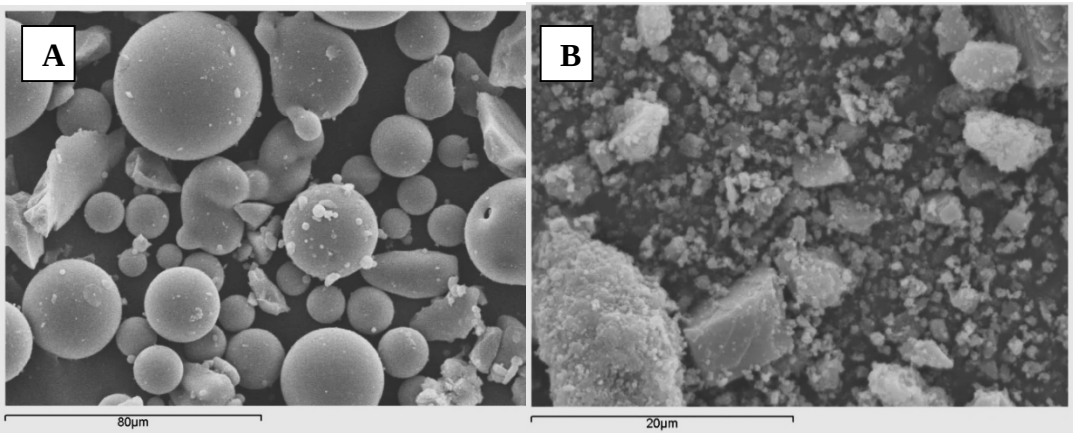


**Figure 9.** Spheriglass (A), $CaCO_3$ (B).

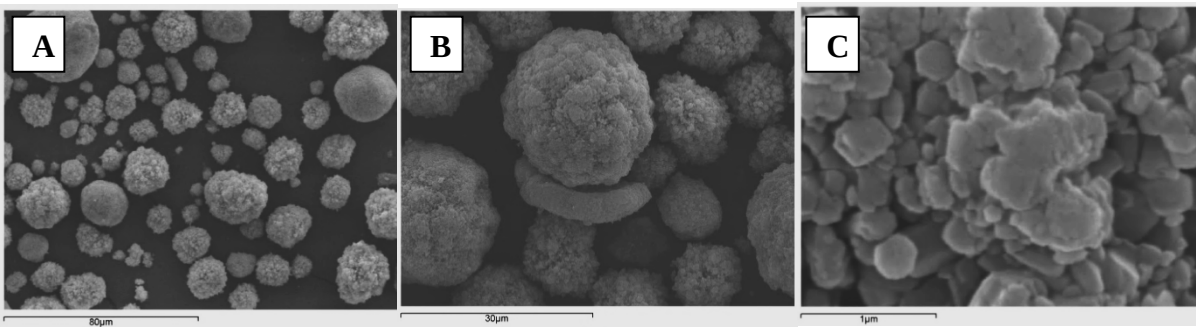


**Figure 10.** HA at low (A), medium (B) and high (C) magnification.

*3.3 Particle Shape Analysis*

The particle shape descriptors of circularity, roundness, Aspect Ratio (AR) and solidity have been evaluated for virgin PA2200, 50/50 virgin/used PA2200, HP3 PEK, PEEK 450PF and 150PF. Circularity evaluates the general shape of a particle. An overall circular polygon has circularity equal to 1, while an elongated shaped element has a value close to zero. Roundness gives information about the edges profile of the particles. Particles with very round edges have values close to one, while values close to zero correspond to very sharp and angular particles. Aspect ratio is the ratio between the major and the minor axes of a particle. Values close to 1 indicate the presence of equiaxed particles that can correspond to different shapes, i.e. circles, squares, overall circular polygons; while higher values identify highly elongated particles. Solidity is the ratio between the measured area of a particle and its corresponding convex area. High values (close to 1) represent very bulky particles, while lower values characterize particles which exhibit irregularities and protuberances on their

surface such as flakes, lumps and outwards elongations. The mean values obtained for the shape descriptors are reported in table 1.

**Table 1.** Shape descriptors average values for PA2200, HP3 PEK, and PEEK grades.

| Material | Circularity | Aspect ratio (AR) | Roundness | Solidity |
|---|---|---|---|---|
| Virgin PA2200 | 0.77 ± 0.11 | 1.51 ± 0.33 | 0.69 ± 0.14 | 0.93 ± 0.03 |
| 50/50 virgin/used PA2200 | 0.81 ± 0.11 | 1.54 ± 0.35 | 0.68 ± 0.14 | 0.94 ± 0.03 |
| HP3 PEK | 0.61 ± 0.18 | 1.83 ± 0.74 | 0.61 ± 0.18 | 0.86 ± 0.09 |
| PEEK 450PF | 0.53 ±0.19 | 2.01 ± 0.84 | 0.57 ± 0.18 | 0.83 ± 0.10 |
| PEEK 150PF | 0.60 ± 0.19 | 1.72 ± 0.61 | 0.63 ± 0.17 | 0.86 ± 0.09 |

Both grades of PA2200 show the highest values of Circularity, Roundness and Solidity and smallest value of AR, suggesting the presence of round, circular, fairly equiaxial and regular (not equipped with flakes and fibrils on their surfaces) particles. HP3 PEK and PEEK 150PF exhibit similar values of Circularity, Roundness and Solidity, which are all lower in comparison with the values for PA2200. Therefore, HP3 PEK and PEEK 150PF powders comprise slightly less round, less circular and less regular particles than PA2200. The lowest values of circularity, roundness, solidity and the highest value of AR occur for PEEK 450PF, implying then the presence of sharper, elongated and irregular particles.

The relationship between circularity and roundness values for a particle has been plotted and presented in figure 11. This graph allows identifying more easily: round and spherical particles (simultaneous high values of circularity and roundness), nearly elliptical particles (low values of circularity and high values of roundness), sharp overall circular shapes (high value of circularity and low value of roundness) and sharp and elongated shapes (low values of both circularity and roundness). The diagrams obtained for the LS materials and PEEK grades are shown in figures 12 and 13. In addition, the Mahalanobis distance, a statistic descriptor able to evaluate the centroid of a data set and the distance of all the data points from it, has been used. More precisely, such distance has been calculated by using the function “Mahal” in the computing software Matlab[51] with number of iterations equal to 300.

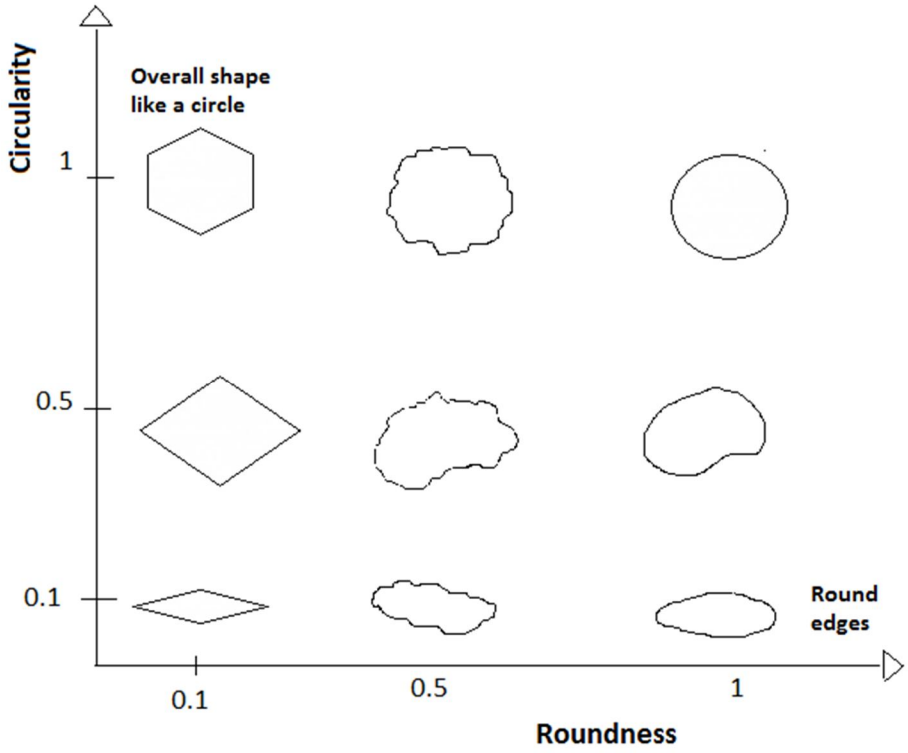


**Figure 11.** Circularity versus Roundness.

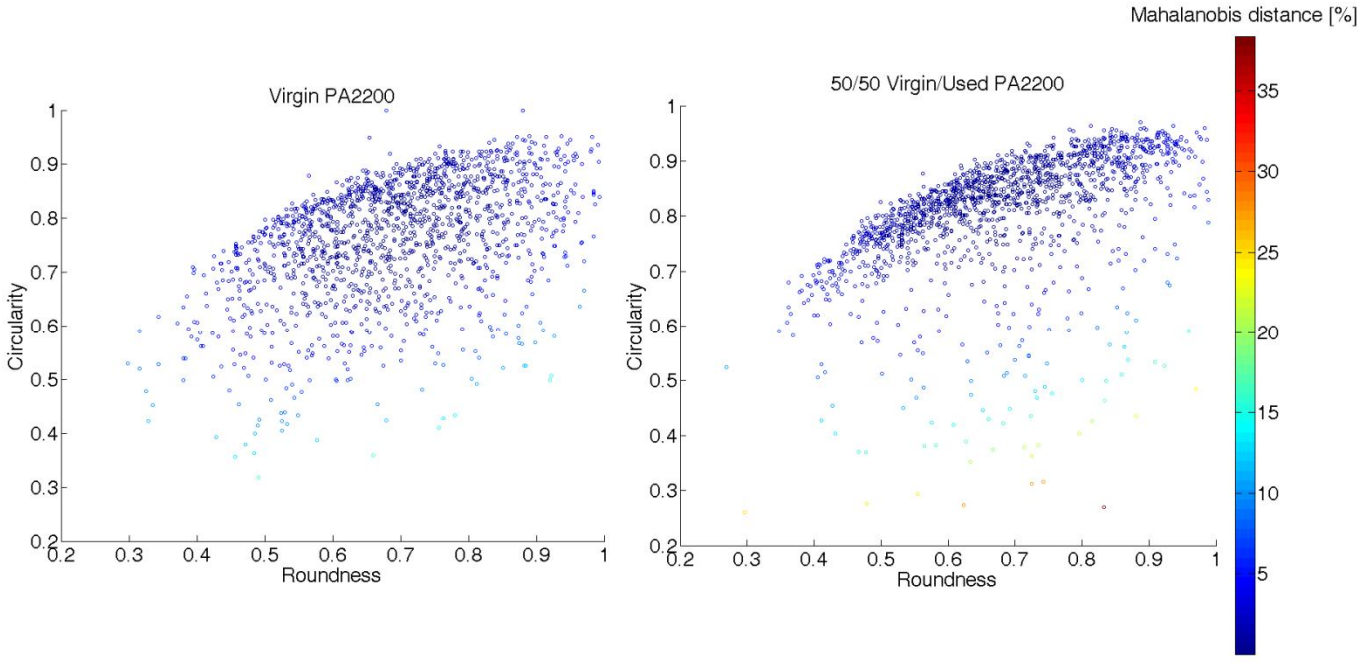


**Figure 12.** Circularity plotted against roundness for virgin PA2200 and 50/50 virgin/used PA2200.

Virgin PA2200 and 50/50 virgin/used PA2200 exhibit datasets centred at high values of roundness and circularity simultaneously. Most particles therefore are confirmed to be round and nearly spherical. It is interesting to notice that particles in 50/50 virgin/used PA2200 are less spread than in virgin PA2200 virgin, indicating a higher circularity and roundness in the particles. In other words, the 50/50 virgin/used PA2200 has better powder qualities.

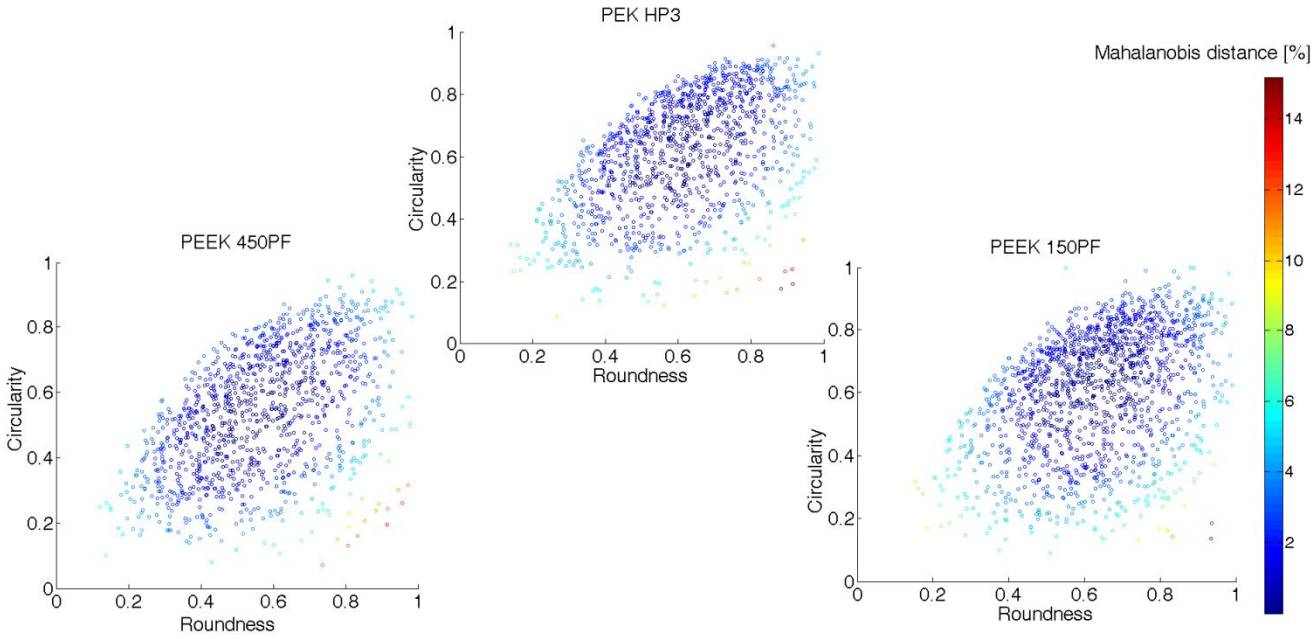


**Figure 13.** Circularity plotted against roundness for HP3 PEK, PEEK 450PF and PEEK 150PF.

The HP3 PEK dataset is centred at middle high values of roundness and circularity, though the data appears more spread towards lower values than in PA2200 grades. PEEK 150PF shows similar results, but slightly shifted towards lower values of circularity. PEEK 450PF shows a data distribution centred just over middle high values of roundness and circularity, indicating a smaller proportion of particles with high values of roundness and circularity compared to PEK HP3 and PEEK 150PF. In order to outline the findings obtained with the Mahalanobis' distance, the centroids of the distributions of each material are reported in figure 14.In agreement with what it was noticed by SEM, the particles of 50/50 virgin/used PA2200 and virgin PA2200 are the most circular and round, where the particles of other grades are less circular, but still have round edges.

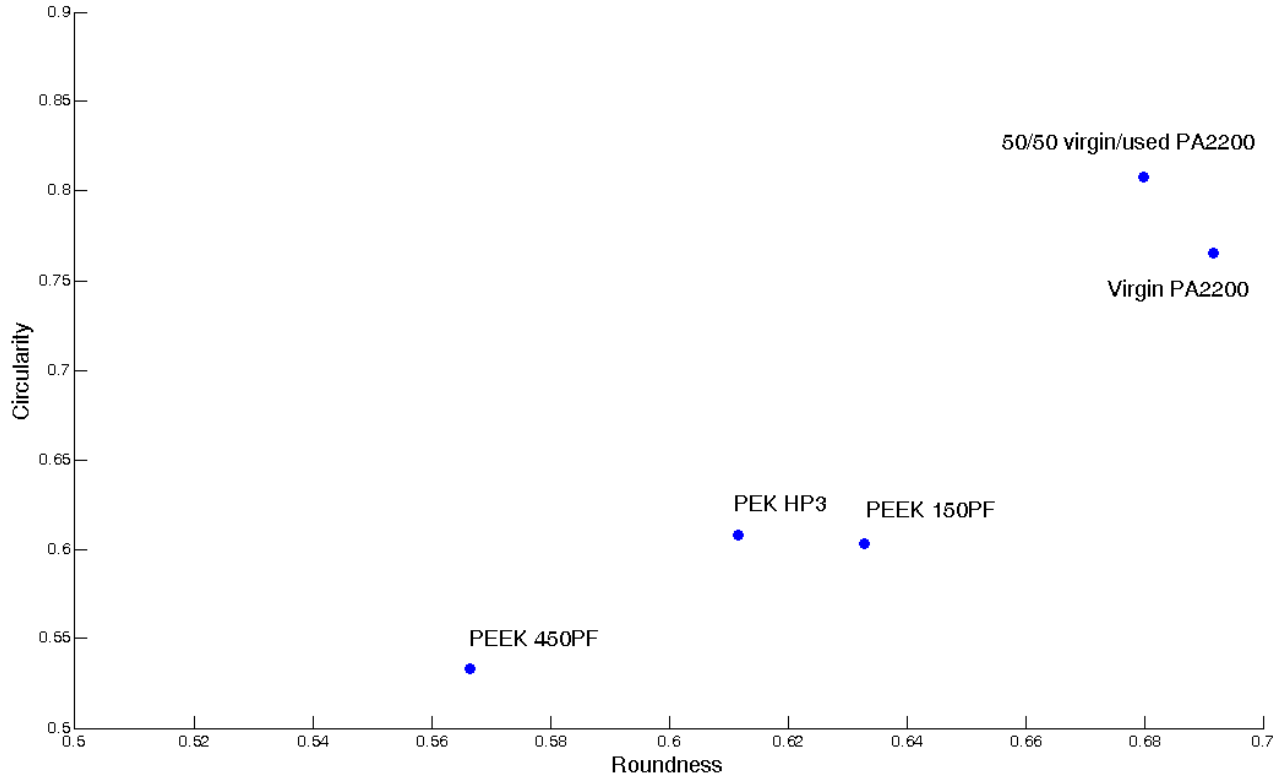


**Figure 14**. Centroids of the Roundness-Circularity distributions.

Data distributions of Aspect Ratio (AR) are reported in figures 15 and 16.

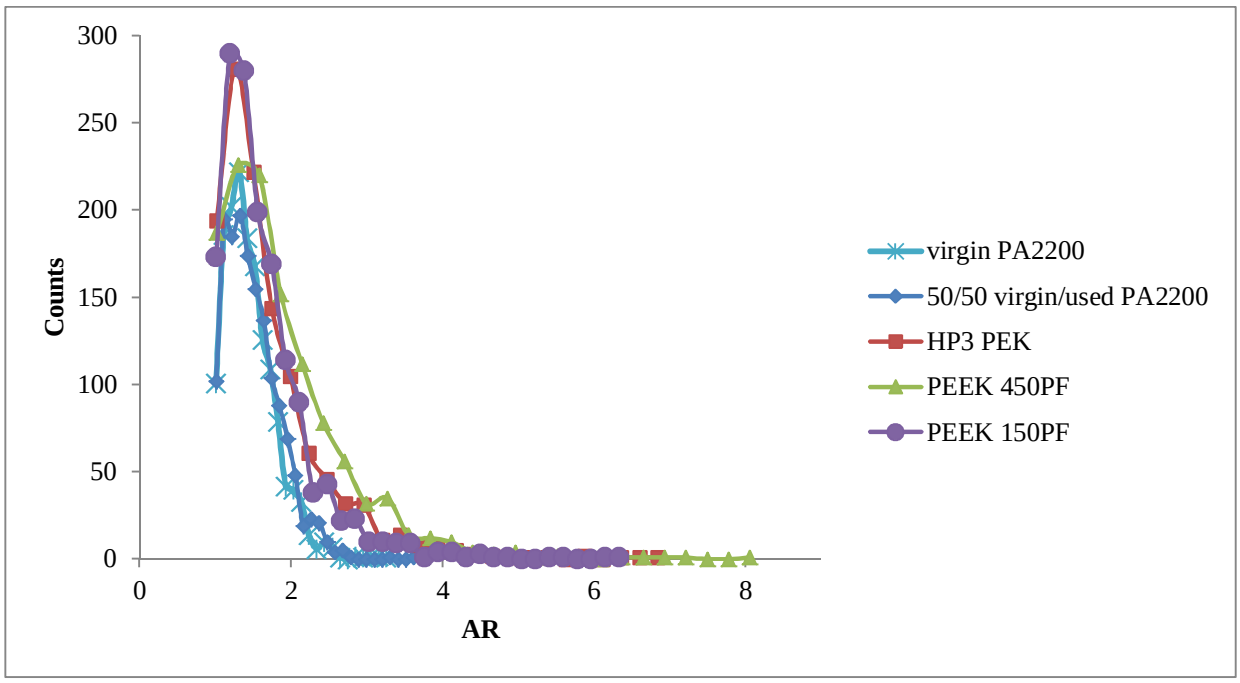


**Figure 15.** Aspect Ratio.

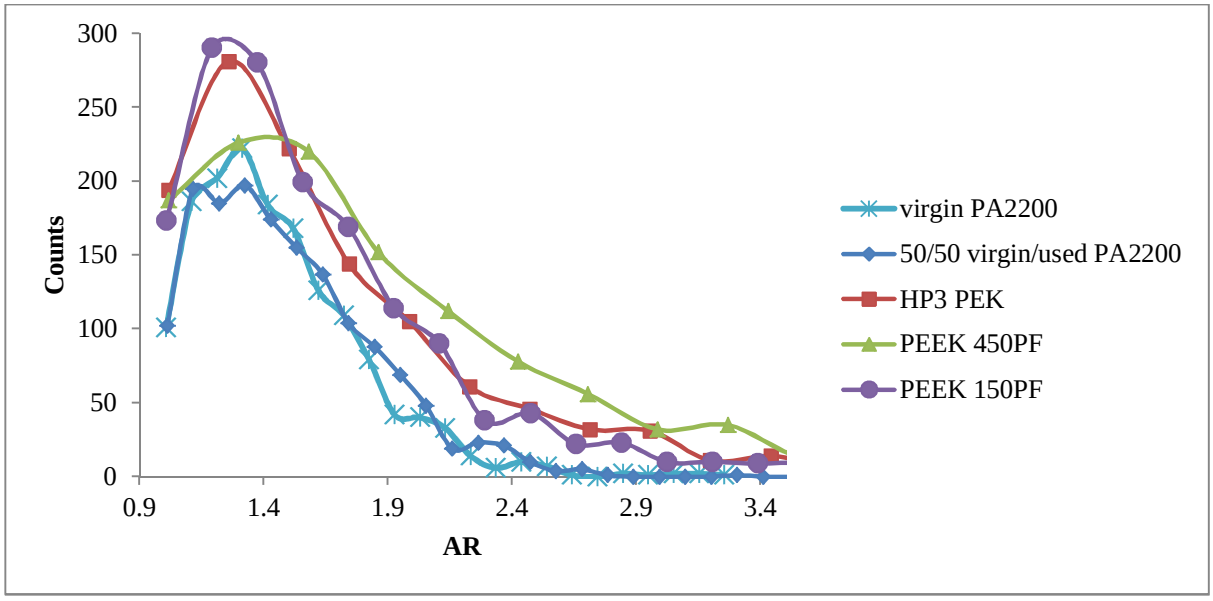


**Figure 16.** Aspect Ratio zoom.

It can be seen that both PA2200 grades exhibit the narrowest distribution among all the materials with values spread between 1.2 and 3.6. More precisely, the highest frequency is slightly over 1.3 indicating that the majority of the particles are circular or slightly elongated. HP3 and PEEK particles show fairly similar distributions, with higher aspect ratio than PA2200. PEEK 450PF powder covers higher values up to 8 (fig. 15), an indication of highly elongated particles compared to the other grades. The experimental results of the descriptor Solidity are showed in figure 17. Again PA2200 grades exhibit the narrowest distribution at higher values of solidity, followed by HP3 PEK, PEEK 150PF and PEEK 450PF. This is not surprising considering the morphological characteristics noticed in figure 6 and 8.The particles are rougher, less round and less circular. It is interesting to notice that 50/50 virgin/used PA2200 used shows higher values of solidity, confirming again the better powder qualities of this material.

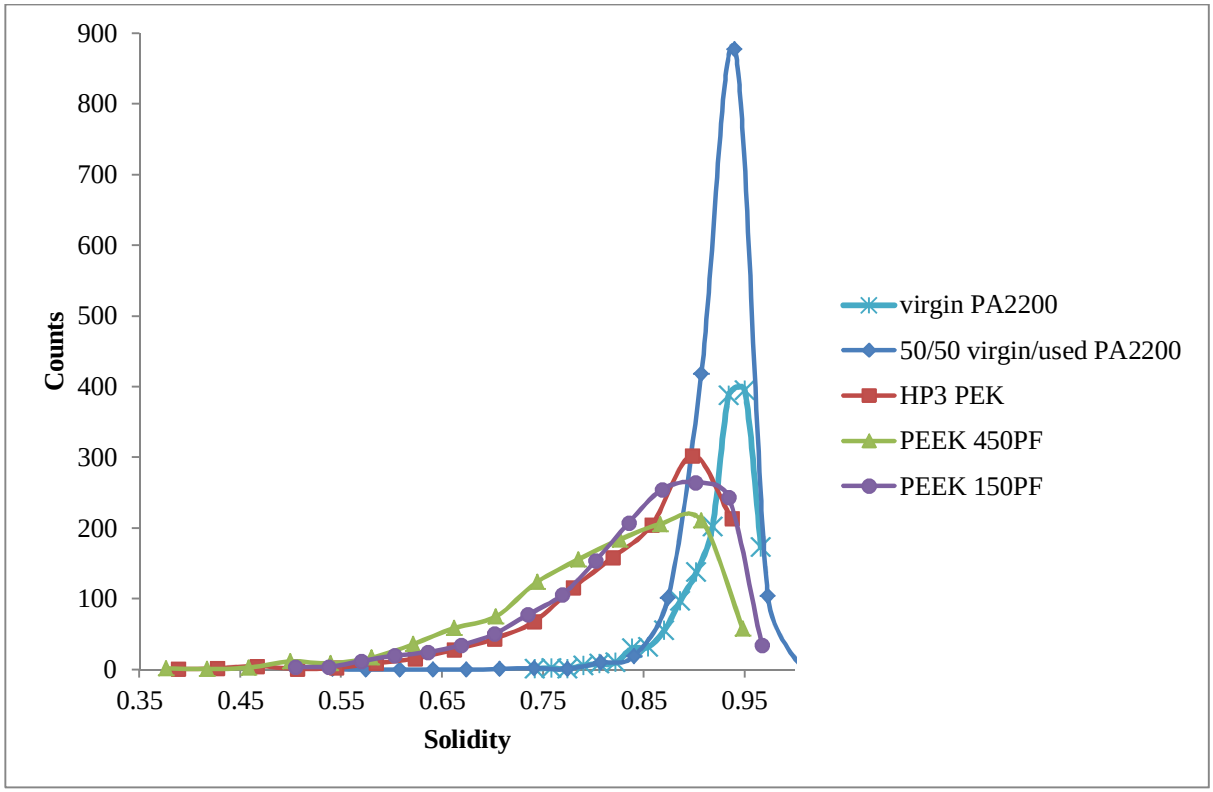


**Figure 17.** Solidity

*3.4 Flowability result*

*3.4.1 Angle of Repose*

The AOR values of commercial LS and non LS grades are reported in table 2, while values of the materials with fillers and additives are reported in table 3.

**Table 2.** AOR values of neat materials

| Material | Angle Of Repose (AOR) ($^0$) |
|---|---|
| Spheriglass | 23.6 ± 1.3 |
| Virgin PA2200 | 33.1 ± 1.5 |
| 50/50 virgin/used PA2200 | 38.4 ± 0.8 |
| HP3 PEK | 42.4 ± 1.1 |
| PEEK 150PF | 47.4 ± 0.7 |
| PEEK 450PF | 52.8 ± 0.9 |

As we move away from Spheriglass and PA2200 which have excellent flow characteristics, the flow performance drops in the PEK and PEEK grades.

**Table 3.** AOR values of fillers and additives

| Material | Angle Of Repose (AOR) ($^0$) |
|---|---|
| (80:20) 450PF/HA | 49.2 ± 1.0 |
| (70:30) 450PF/ HA | 50.4 ± 0.7 |
| (90:10) 450PF/$CaCO_3$ | 50.3 ± 1.0 |
| (80:20) 450PF/$CaCO_3$ | 49.4 ± 0.7 |
| (70:30) 450PF/$CaCO_3$ | 48.2 ± 1.0 |
| (90:10) 450PF/Spheriglass | 51.8 ± 0.8 |
| (80:20) 450PF/Spheriglass | 50.0 ± 0.9 |
| (70:30) 450PF/Spheriglass | 48.6 ± 1.7 |
| (99:1) 450PF/Aerosil | 43.0 ± 0.4 |
| (99:1) 150PF/Aerosil | 36.4 ± 0.5 |

Several studies in the literature [21, 52-55] discuss the incorporation of additives to improve the flow of new powders for LS applications. In most cases, the addition of small quantities of powders seems to improve flowability although the mechanisms leading to this improvement are never discussed and no results are presented to support their proposals.

It is believed that, depending on the particle size, these additives can enhance the flow performance of the PEEK 450PF in two ways: they either mechanically engage the polymeric particles in the flow when the additives have a similar particle size as the host powder; or when additives have such small particles that they fill in the spaces between the surface flakes and fibrils and the main body of the particle, leading to less inter-linking and agglomerations of the particles and therefore better flow. Such hypothesis is supported by the image of PEEK 450PF/$CaCO_3$ (70:30) (Fig.18).The smaller particles of $CaCO_3$ are located in the empty spaces created by the flakes on the surfaces of the PEEK 450PF particles, filling in the gaps and acting as interspacing. It is believed that the flakes help the particles interlock and drag each other into agglomerates, which spread more difficultly as a result.

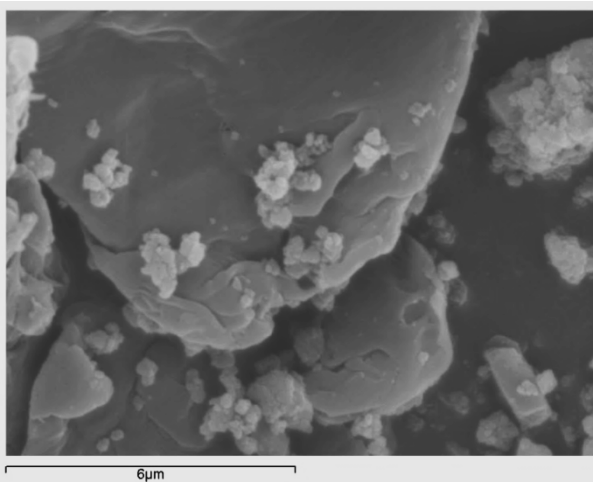


**Figure 18.** 70:30 450PF/$CaCO_3$ [56].

Adding the glass particles to PEEK 450PF caused a slight decrease in the AOR value and therefore an increase of the flow performance, as expected from the corresponding SEM images. Similarly, the addition of HA particles to PEEK 450PF improved the flow property only at the lowest concentration (20%). This could be due to the complex structure of HA particles, which instead of facilitating reciprocal sliding of the particles caused more inter-particle mechanical locking due to the surface roughness (see Fig. 10). In both cases, glass and hydroxyapatite, it was surprising to see that these particles although round do not necessary help the flow in spite of their high concentrations in the mix. Interestingly, the addition of $CaCO_3$ powder makes the polymeric powder flow best, increase of concentration leading to a lower AOR and therefore better flow. It is then possible to say that both adding smooth and round particles (Spheriglass) but with size comparable to the PEEK 450PF particles and incorporating smaller and rounder particles (HA and $CaCO_3$) slightly improved the flow.

The incorporation of the nano flow aid powder Aerosil Pharma 200 to PEEK 450PF and 150PF reduced the AOR by 10˚ or more. This is not surprising as the van der Waals forces between two spheres decrease when one of them is significantly smaller than the other one[37].

*3.4.2 Hamaker constant results*

The Hamaker constant results (A) of the pure materials are reported in table 4. Spheriglass 2000 and PA2200 are characterized by the lowest values of Hamaker constants (smaller interparticle interactions) which confirms the better flow performances arisen from the AOR tests. In table 5, values for PEEK, fillers and additives are reported. PEEK with Aerosil Pharma 200 presents the lowest value, followed by the combination with Spheriglass, $CaCO_3$ and HA. The effect of viscosity on the dielectric constants and refractive indices measurements has not been considered here, one

literature value [46, 57] has been used for the calculation of the Hamaker constants for PEEK and PEEK blends. The results agree with the findings found for AOR, i.e. the materials with higher values of AOR showed greater values of Hamaker constant. In addition, the same order of performance across the materials is confirmed in the Hamaker constants.

**Table 4.** Hamaker values of pure materials

| Materials ( in air) | A (J) |
|---|---|
| PEEK-PEEK | $1.26 \times 10^{-19}$ |
| Polyamide 12 - Polyamide 12 | $7.65 \times 10^{-20}$ |
| Spheriglass -Spheriglass | $7.44 \times 10^{-20}$ |

**Table 5.** Hamaker values of PEEK with fillers and additives

| Mixtures (in air) | A (J) |
|---|---|
| Aerosil - PEEK | $8.67 \times 10^{-20}$ |
| Spheriglass – PEEK | $9.67 \times 10^{-20}$ |
| $CaCO_3$ - PEEK | $1.06 \times 10^{-19}$ |
| HA - PEEK | $1.18 \times 10^{-19}$ |

## 4. Conclusions

Polymeric LS is a manufacturing process whose potential may become limited by the small range of powder materials currently available and the general lack of their characterization. Therefore quantitative analyses on existing LS materials and new candidates for LS are presented here with special attention to the flow performance, one of the first operation steps during a LS manufacturing process. The PSD results revealed similar trends for the LS and non-LS polymeric powder grades; however the angle of repose, the shape analysis and the Hamaker constants led to different findings. The AOR for the commercially used LS grades was found to be between 33 and 42, where the non-LS grades gave higher AOR values. SEM analysis showed morphological differences between the grades and explained the differences in the AOR results. Although the presence of fillers slightly improved the AOR independently of their particle size distribution, the nano-sized additive improved the flowability significantly. The shape analysis outlined that middle to high values of Roundness and Circularity, coupled with high values of Solidity and middle to low values of Aspect Ratio are

characteristic of the commercial LS materials such as PA2200 and PEK HP3. Lastly, the estimation of Hamaker constants confirmed the findings of the AOR tests, and pointed out that, in addition to the particle size and morphology, the physicochemical nature of the materials has an important effect on the flow performance. The data showed here constitute a starting point in a quantitative characterization and understanding of powder materials for LS. The study showed that the non-commercial PEEK grades require optimization that can be achieved through tempering methods [58] and incorporation of nano additives. In addition, powder characteristics and optimization treatments cannot be considered in isolation; further investigation into spreading and processability of the powders in the actual sintering system needs to be carried out for a full assessment of a specific material.

## 5. Acknowledgments

The authors wish to acknowledge the support of Invibio® Biomaterial Solutions[44] for the supply of materials and especially Andy Anderson for the technical assistance during the preparation of the paper.

## 6. References

1. Goodridge, R.D., R.J.M. Hague, and C.J. Tuck, *An empirical study into laser sintering of ultra-high molecular weight polyethylene (UHMWPE).* Journal of Materials Processing Technology, 2010. **210**(1): p. 72-80.
2. Goodridge, R.D., R.J.M. Hague, and C.J. Tuck, *Effect of long-term ageing on the tensile properties of a polyamide 12 laser sintering material.* Polymer Testing, 2010. **29**(4): p. 483-493.
3. Goodridge, R.D., et al., *Processing of a Polyamide-12/carbon nanofibre composite by laser sintering.* Polymer Testing, 2011. **30**(1): p. 94-100.
4. Goodridge, R.D., C.J. Tuck, and R.J.M. Hague, *Laser sintering of polyamides and other polymers.* Progress in Materials Science, 2012. **57**(2): p. 229-267.
5. Zarringhalam, H., et al., *Effects of processing on microstructure and properties of SLS Nylon 12.* Materials Science and Engineering: A, 2006. **435–436**: p. 172-180.
6. Athreya, S.R., K. Kalaitzidou, and S. Das, *Mechanical and microstructural properties of Nylon-12/carbon black composites: Selective laser sintering versus melt compounding and injection molding.* Composites Science and Technology, 2011. **71**(4): p. 506-510.
7. Truss, R.W., et al., *Cold compaction molding and sintering of ultra high molecular weight polyethylene.* Polymer Engineering & Science, 1980. **20**(11): p. 747-755.
8. Olinek, J., C. Anand, and C.T. Bellehumeur, *Experimental study on the flow and deposition of powder particles in rotational molding.* Polymer Engineering & Science, 2005. **45**(1): p. 62-73.
9. Schultz J.P., M.J.P., Kander R.G. and Suchital T.A., *Selective Laser Sintering of Nylon 12-PEEK Blends Formed by Cryogenic Mechanical Alloying*, in *International Solid Freeform Fabrication Symposium* 2000: Austin (TX), USA.
10. Prescott J.K., B.R.A., *On powder flowability.* Pharmaceutical Technology, 2000. **October 2010**

11. Schulze, D., *Flow Properties of Powders and Bulk Solids*, 2006-2011.
12. Nelson, J.C., et al., *Model of the selective laser sintering of bisphenol-A polycarbonate.* Industrial & Engineering Chemistry Research, 1993. **32**(10): p. 2305-2317.
13. Butscher, A., et al., *Structural and material approaches to bone tissue engineering in powder-based three-dimensional printing.* Acta Biomaterialia, 2011. **7**(3): p. 907-920.
14. Forderhase P. , M.K., Booth . *The development of a SLS® composite material.* Proceedings of the Solid Freeform Fabrication Symposium, 1995: p. 287–297.
15. Chung, H. and S. Das, *Processing and properties of glass bead particulate-filled functionally graded Nylon-11 composites produced by selective laser sintering.* Materials Science and Engineering: A, 2006. **437**(2): p. 226-234.
16. Drummer, D., D. Rietzel, and F. Kühnlein, *Development of a characterization approach for the sintering behavior of new thermoplastics for selective laser sintering.* Physics Procedia, 2010. **5, Part B**: p. 533-542.
17. Gibson, I. and D.P. Shi, *Material properties and fabrication parameters in selective laser sintering process.* Rapid prototyping journal, 1997. **3**(4): p. 129-136.
18. Xiao, K., et al., *Indirect selective laser sintering of apatite—wollostonite glass—ceramic.* Proceedings of the Institution of Mechanical Engineers, Part H: Journal of Engineering in Medicine, 2008. **222**(7): p. 1107-1114.
19. McAlea, K., *Selective Laser Sintering Of Polymer Powder Of Controlled Particle Size Distribution*, 1998.
20. Hao, L., et al., *Characterization of selective laser-sintered hydroxyapatite-based biocomposite structures for bone replacement.* Proceedings of the Royal Society A: Mathematical, Physical and Engineering Science, 2007. **463**(2084): p. 1857-1869.
21. Tan, K.H., et al., *Scaffold development using selective laser sintering of polyetheretherketone–hydroxyapatite biocomposite blends.* Biomaterials, 2003. **24**(18): p. 3115-3123.
22. Tan, K.H., et al., *Selective laser sintering of biocompatible polymers for applications in tissue engineering.* Bio-Medical Materials and Engineering, 2005. **15**(1-2): p. 113-124.
23. Tan, K.H., et al., *Fabrication and characterization of three-dimensional poly(ether-ether-ketone)/-hydroxyapatite biocomposite scaffolds using laser sintering.* Proceedings of the Institution of Mechanical Engineers, Part H: Journal of Engineering in Medicine, 2005. **219**(3): p. 183-194.
24. Van der Schueren B., K.J.P., *Powder deposition in selective metal powder sintering.* Rapid Prototyping Journal Volume 1 · Number 3 · 1995 · pp. 23–31, 1995.
25. Dupin, S., et al., *Microstructural origin of physical and mechanical properties of polyamide 12 processed by laser sintering.* European Polymer Journal.
26. Amado, A., Schmid, M., Levy, G. & Wegener, K., *Advances in SLS Powder Characterization*, in *Proceedings SFF Symposium*2011: Austin, Texas. p. 438-452.
27. EOS, *http://www.eos.info/en/home.html.*
28. Beard, M.A., et al., *Material characterisation of Additive Manufacturing components made from a polyetherketone (PEK) high temperature thermoplastic polymer*, in *Innovative Developments in Virtual and Physical Prototyping*2011, CRC Press. p. 329-332.
29. Victrex. *http://www.victrex.com*.
30. Potters. *http://pottersbeads.com/*.
31. Aldrich, S. *http://www.sigmaaldrich.com/sigma-aldrich/home.html*.
32. Grove, A. *http://www.ashgrove.com/*.
33. Evonik. *http://corporate.evonik.com/en/Pages/default.aspx*.
34. NHS. *Image J*. Available from: http://rsbweb.nih.gov/ij/.
35. ASTM, *ASTM C 1444 – 00 Standard Test Method for Measuring the Angle of Repose of Free-Flowing Mold Powders*.

36. Ileleji, K.E. and B. Zhou, *The angle of repose of bulk corn stover particles.* Powder Technology, 2008. **187**(2): p. 110-118.
37. Seville, J.P., R. Clift, and U. Tüzün, *Processing of Particulate Solids* 2011: Springer London, Limited.
38. Hamaker, H.C., *The London—van der Waals attraction between spherical particles.* Physica, 1937. **4**(10): p. 1058-1072.
39. Lomboy, G., et al., *A test method for determining adhesion forces and Hamaker constants of cementitious materials using atomic force microscopy.* Cement and Concrete Research, 2011. **41**(11): p. 1157-1166.
40. Huang, Q., et al., *Measurement of inter-particle forces by an interfacial force microscope.* Particuology, 2010. **8**(5): p. 400-406.
41. Das S., S.P.A., Raychaudhuri R.K., *A method to quantitatively evaluate the Hamaker constant using the jump-into-contact effect in atomic force microscopy* Nanotechnology, 2007. **18**.
42. Argento C., F.R.H., *Parametric tip model and force–distance relation for Hamaker constant determination from atomic force microscopy.* Journal of Applied Physics, 1996. **80**(11).
43. Israelachvili, J.N., *Intermolecular and Surface Forces: Revised Third Edition*2011: Elsevier Science.
44. Invibio. *http://www.invibio.com/*.
45. Matweb. *http://www.matweb.com/*.
46. TWI, *http://www.twi.co.uk/news-events/bulletin/archive/2004/may-june/polymer-performance-in-a-tough-world/*.
47. Goyal R.K., S.J.N., *Fabrication of advanced poly(etheretherketone)/clay nanocomposites and their properties.* Adv. Mat. Lett, 2010. **1**(3): p. 205-209.
48. http://www.spacekdet.com/tutorials/IOR.html.
49. http://www.rafoeg.de/20, D., Daten/dielectric_chart.pdf.
50. Evans, R.W., H.S. Cheung, and D.J. McCarty, *Cultured canine synovial cells solubilize 45Ca-labeled hydroxyapatite crystals.* Arthritis & Rheumatism, 1984. **27**(7): p. 829-832.
51. MATLAB. *http://www.mathworks.co.uk/products/matlab/*.
52. Pohle, D., et al., *Processing of Three-Dimensional Laser Sintered Polyetheretherketone Composites and Testing of Osteoblast Proliferation in vitro.* Macromolecular Symposia, 2007. **253**(1): p. 65-70.
53. Schmidt, M., D. Pohle, and T. Rechtenwald, *Selective Laser Sintering of PEEK.* CIRP Annals - Manufacturing Technology, 2007. **56**(1): p. 205-208.
54. von Wilmowsky, C., et al., *Effects of bioactive glass and β-TCP containing three-dimensional laser sintered polyetheretherketone composites on osteoblasts in vitro.* Journal of Biomedical Materials Research Part A, 2008. **87A**(4): p. 896-902.
55. Von Wilmonsky, C., et al., *In Vivo Evaluation of ß-TCP Containing 3D Laser Sintered Poly(ether ether ketone) Composites in Pigs.* Journal of Bioactive and Compatible Polymers, 2009. **24**(2): p. 169-184.
56. Berretta S., G.O., Evans K.E., Anderson A. and Newman C. *Size, shape and flow of powders for use in Selective Laser Sintering (SLS)* in *Advanced research in virtual and rapid prototyping*. 2013. Leiria, Portugal: CRC Press.
57. Biron, M. and O. Marichal, *Thermoplastics and Thermoplastic Composites*2012: William Andrew.
58. Leuterer M., M.F., Pfister A., *PAEK powder, in particular for the use in a method for a layer-wise manufacturing of a three-dimensional object, as well as method for producing it*, 2012.